ScienceAdvances

www.advances.sciencemag.org/cgi/content/full/1/4/e1500014/DC1

Supplementary Materials for

Northwestern Pacific typhoon intensity controlled by changes in ocean temperatures

Wei Mei, Shang-Ping Xie, François Primeau, James C. McWilliams, Claudia Pasquero

Published 29 May 2015, *Sci. Adv.* **1**, e1500014 (2015)
DOI: 10.1126/sciadv.1500014

This PDF file includes:

Supplementary Materials and Methods

Sensitivity test using best track data from Japan Meteorological Agency

The Japan Meteorological Agency (JMA) provides maximum 10-minute sustained wind speed (MSW_{10min}) starting from 1977, while the Joint Typhoon Warning Center (JTWC) provides maximum 1-minute sustained wind speed (MSW_{1min}). To facilitate the comparison, we first converted the JMA MSW_{10min} to MSW_{1min}. Note that JMA employed different methodologies to estimate MSW_{10min} between 1977 and 2010 (*80*). Prior to 1987, MSW_{1min} was estimated first and then converted to MSW_{10min} using a linear relationship. After that, MSW_{10min} was directly estimated using the Dvorak technique and the current intensity number-maximum wind speed relationship based on Koba table (*81*).

We converted MSW_{10min} to MSW_{1min} using a method consistent over the entire period. Prior to 1987, we obtained MSW_{1min} by dividing MSW_{10min} by 0.88 (e.g., (*82*)). After 1987, we first converted MSW_{10min} to Dvorak current intensity number using the Koba table, and then calculated MSW_{1min} using the Dvorak table (*83*).

We then repeated the calculations in the main text using this adjusted JMA MSW_{1min} dataset. The results for various typhoon metrics (including seasonal-mean lifetime peak intensity, intensification rate, and intensification duration) are generally consistent with those based on the JTWC data with a linear correlation coefficient of 0.6-0.8. As an example, fig. **S1** shows the temporal evolution of seasonal-mean typhoon lifetime peak intensity calculated using the JTWC data and the new JMA MSW_{1min} data. The results from the two datasets are very similar with a correlation coefficient of 0.72. They also exhibit nearly identical linear trend between 1977 and 2010. The positive trend in typhoon intensity is in line with the recent modeling studies (e.g., (*84*)) and with the analyses from independent meteorological and oceanographic datasets by (*29*), although the trend is insignificant in the intensity data of (*85*) and in lifetime mean intensity of (*86*) estimated from minimum central pressure.

Sensitivity analyses for changes in intensity measurements

Measurements of TC intensity have evolved with time over the northwestern Pacific. Before early 1970s, reliable intensity estimates were mainly obtained from aircraft reconnaissance. After that, global satellite observations together with pattern recognition intensity estimates based on the Dvorak technique (*83*) have become essential for intensity measurements, with aircraft reconnaissance providing fixes and calibrations until 1987 (*87*). Thus we preformed following sensitivity tests. Firstly, we tested the results using intensity data only during the recent three decades. We found that the relationship between intensification rate and ocean temperatures and that between intensification duration and ENSO/PDO keep nearly unchanged. Secondly, because the observations and techniques evolve on a relatively slow time scale, we recalculated the correlation coefficients after removing the low-frequency variations in both typhoon metrics and oceanic and climate variables. The results are basically the same (fig. **S8**). Furthermore, the intensity data from the JTWC and JMA are generally consistent (fig. **S1**). All of these examinations suggest that our results are robust.

In addition, we note that continuous improvements in satellite resolution in more recent

decades may have improved intensity estimates, whereas the termination of aircraft reconnaissance in 1987 may have degraded intensity observations (*88, 89*). The two factors oppose each other in intensity estimates, and the degree of offsetting is difficult to quantify.

A discussion on the potential lapse rate effect

In this study, our statistical model may omit some physical processes that are insignificant in current climate variability but may become important for typhoon intensification under global warming. In particular, modeling studies suggest that the thermal lapse rate decrease suppresses TC intensification in a warming climate (*60, 61*). We have calculated the correlation between typhoon intensification rate and the lapse rate [defined as the temperature difference between 1000 and 300 hPa as in (*60*)] averaged over the intensification region between 1979 and 2009. The result ($r = -0.32$) appears to be counterintuitive since it implies that an increased stability favors stronger intensification. Under global warming such a negative relationship may exist, as SST warming increases intensification rate and is accompanied by a reduced lapse rate and meanwhile the intensification induced by SST warming exceeds the mitigating effect of lapse rate decrease (*60, 61*). No significant correlation, however, is found between SST and lapse rate ($r = 0.04$) during 1979-2009, when SST has a positive trend and lapse rate shows no significant trends. This together with the marginally significant correlation between intensification rate and lapse rate prompts us to interpret this correlation as a coincidence instead of causality, and it is very likely that current observations do not sample the lapse rate effect on typhoon intensification. Moreover, the variation in lapse rate under current climate is quite small with a standard deviation of $\sim$0.25°C. The induced intensification rate change based on refs. (*60, 61*) is $\sim$0.08 m s^{-1} per 6 hr, which is nearly one order of magnitude smaller than the observed changes in intensification rate whose standard deviation is $\sim$0.6 m s^{-1} per 6 hr. This further justifies our omission of the lapse rate effect in our statistical model for the period when observations are available.

In a warming climate, a significant reduction in the thermal lapse rate due to the stronger warming in the upper troposphere than the lower troposphere (green curve in fig. **S9**) is expected to suppress TC intensification based on the above-mentioned modeling studies (*60, 61*). The concurrent increase in moist instability caused by pronounced moistening of the lower troposphere (red curve in fig. **S9**), however, favors TC intensification. Similar to the lapse rate effect, we could not quantify the moist instability effect on TC intensification using current observations [The correlation coefficient between typhoon intensification rate and 1000–500-hPa θ_e difference (*90*) is -0.12 during 1979-2009]. It is likely that the SST effect represented in our statistical model may not include the moist instability effect or include only part of it. If the unrepresented part dominates over the lapse rate effect, then changes in the atmospheric thermodynamic profile under global warming will be a further enhancement to TC intensification, beyond the effect we have focused on of ocean/SST warming (mainly through enhanced air-sea enthalpy flux). Those two opposing factors may bring uncertainty to the size of our projected typhoon intensity increase, which needs further exploration, but we think their inclusion should not change our main conclusion given the overwhelming role of SST warming and enhanced

air-sea enthalpy flux.

Supplementary Figures

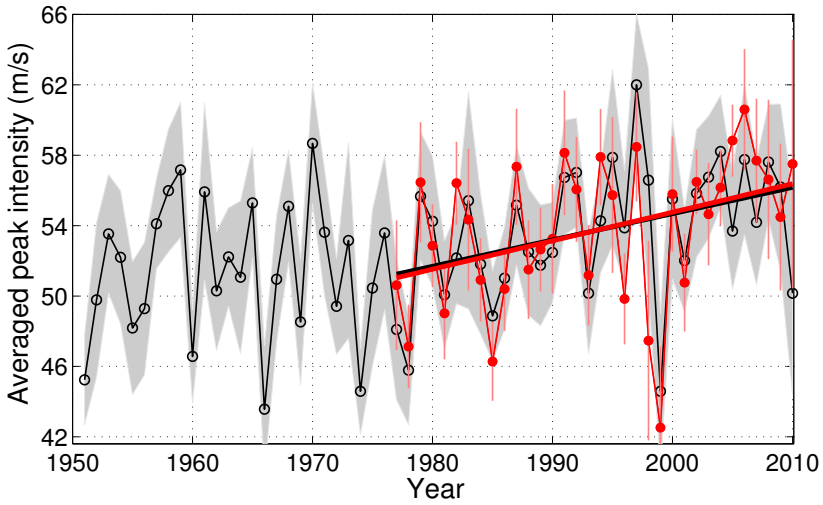

Fig. S1. **Evolution of seasonal-mean lifetime peak intensity of typhoons.** Temporal evolution of seasonal-mean lifetime peak intensity of typhoons in the northwestern Pacific calculated using data from the Joint Typhoon Warning Center (thin black curve; same as in Fig. **1**A) and using the recovered data from the Japan Meteorological Agency (thin red curve). The red curve has been shifted upward by 2.25 m s^{-1} to offset the difference in the mean value of the two curves between 1977 and 2010. Gray shading and vertical light-red lines show their respective error bars. The thick black and red lines respectively show their linear trends between 1977 and 2010. The correlation coefficient between the two thin curves during 1977-2010 is 0.72.

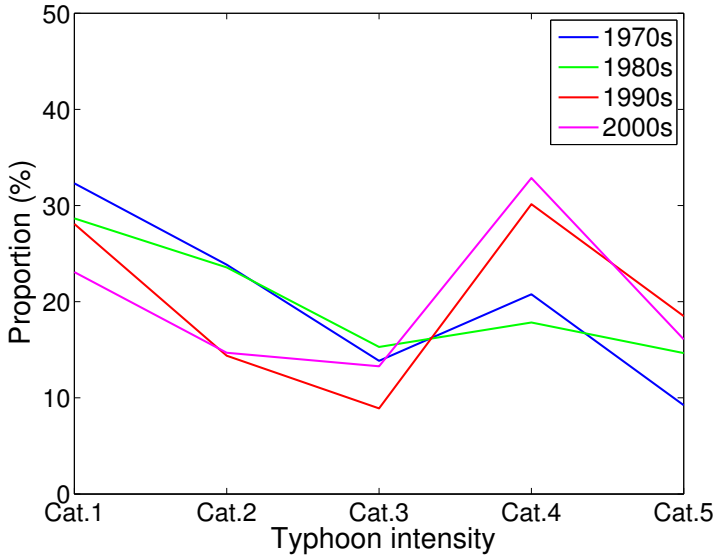

Fig. S2. **Changes in proportions of TCs of different intensity.** Changes in proportions of TCs of different intensity relative to the total typhoons in the northwestern Pacific.

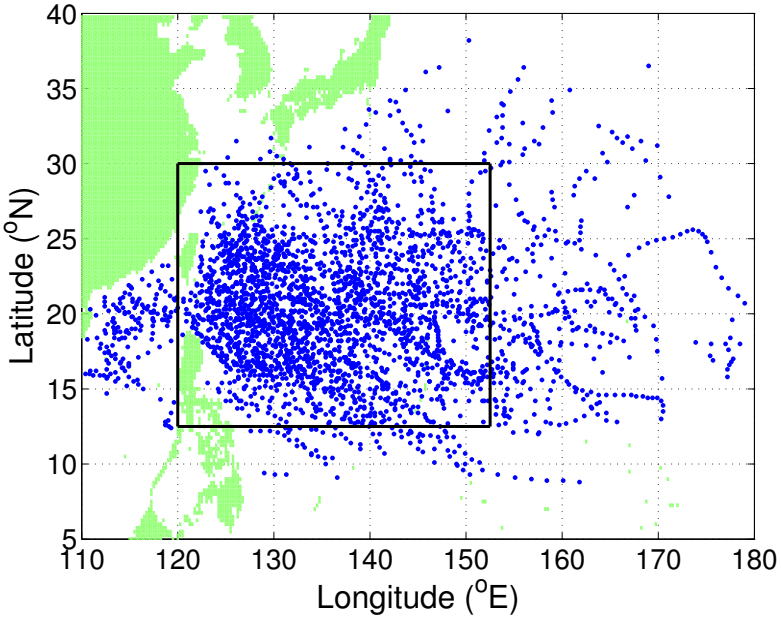

Fig. S3. **Main typhoon intensification region.** Geographic distribution of the locations where the typhoon intensification occurs during the typhoon peak season (July–September). The thick black lines identify the main intensification region used in this study.

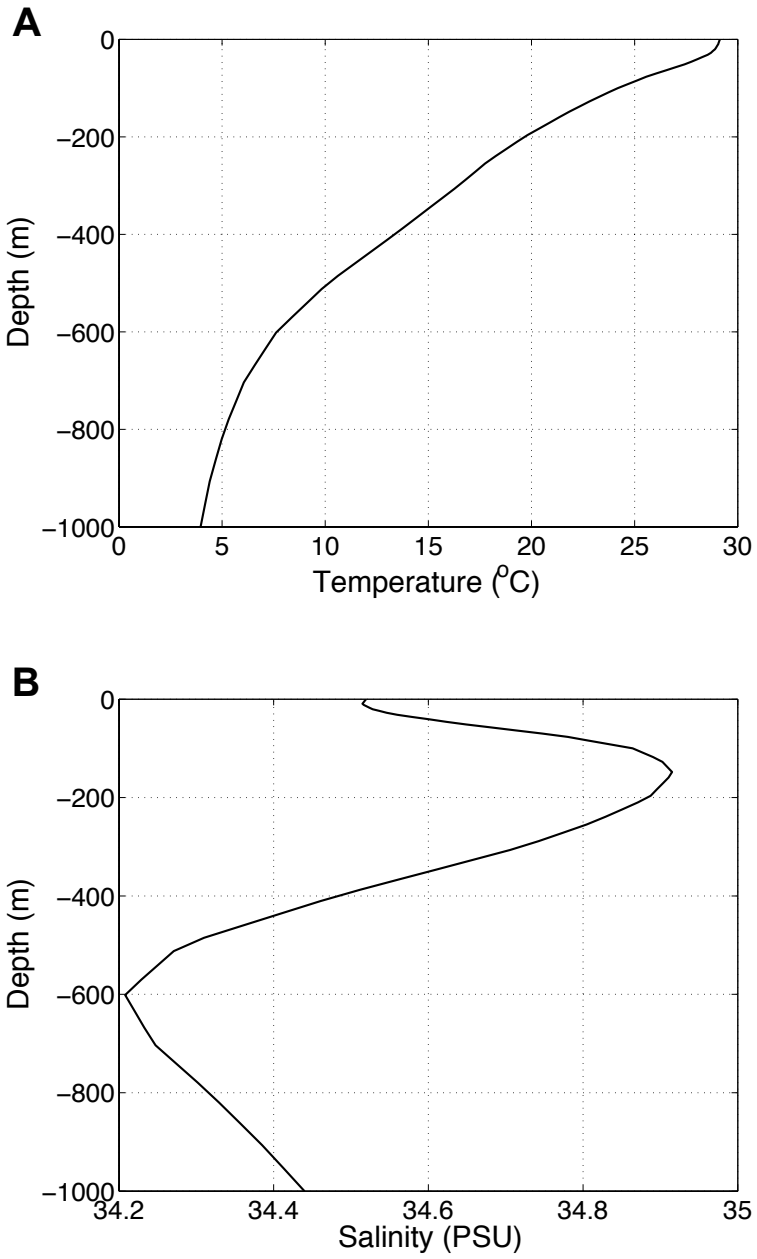

Fig. S4. **Vertical profiles of temperature and salinity used to initialize the ROMS simulation.** (A) temperature and (B) salinity. These profiles are obtained from WOA09.

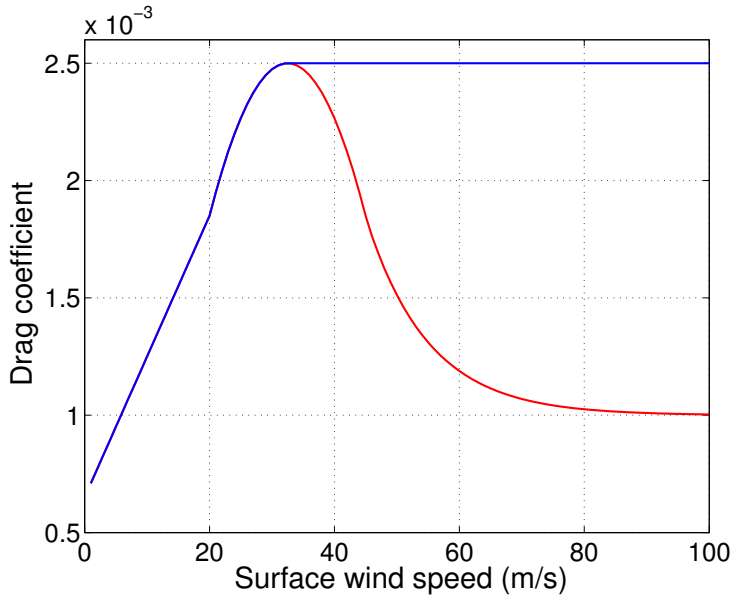

Fig. S5. **Drag coefficient as a function of surface wind speed used in ROMS simulations.** The one shown in red is adapted from (*78*) (see the red curve in their Fig. 3), and the other shown in blue is very similar to the estimates by (*79*) (see their Fig. 2).

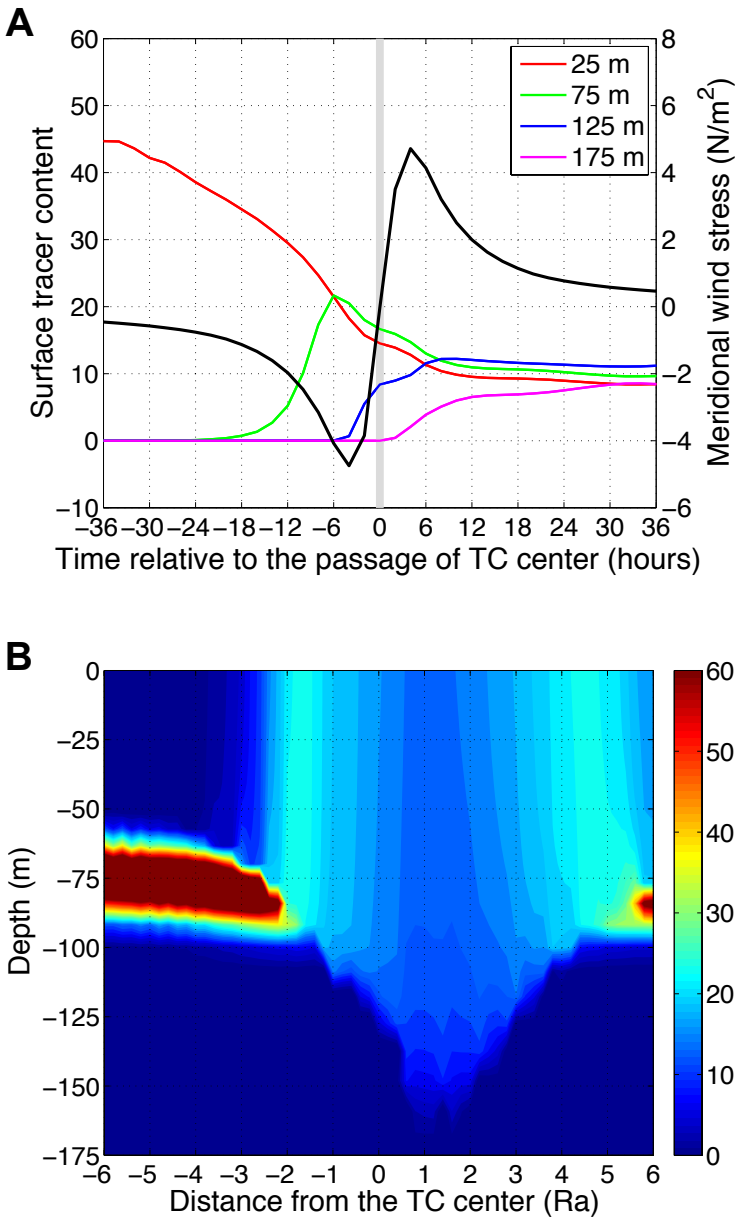

Fig. S6. **Typhoon-induced changes in tracer content simulated by ROMS.** (A) Temporal evolution of the surface concentration of tracers at a fixed location on the typhoon track relative to the typhoon passage. The tracers are initialized at various depths–25 m (red curve), 75 m (green curve), 125 m (blue curve), and 175 m (magenta curve)–three days before the typhoon passage. Also plotted is the evolution of the meridional wind stress at the same location (black curve; right y axis) to indicate the typhoon passage. Vertical thick gray line indicates the time of typhoon passage. (B) Cross-track and vertical section of the concentration of a passive tracer that is initially located around 75 m depth during the typhoon passage. The unit of the horizontal axis is the radius of maximum wind speed (i.e., 50 km).

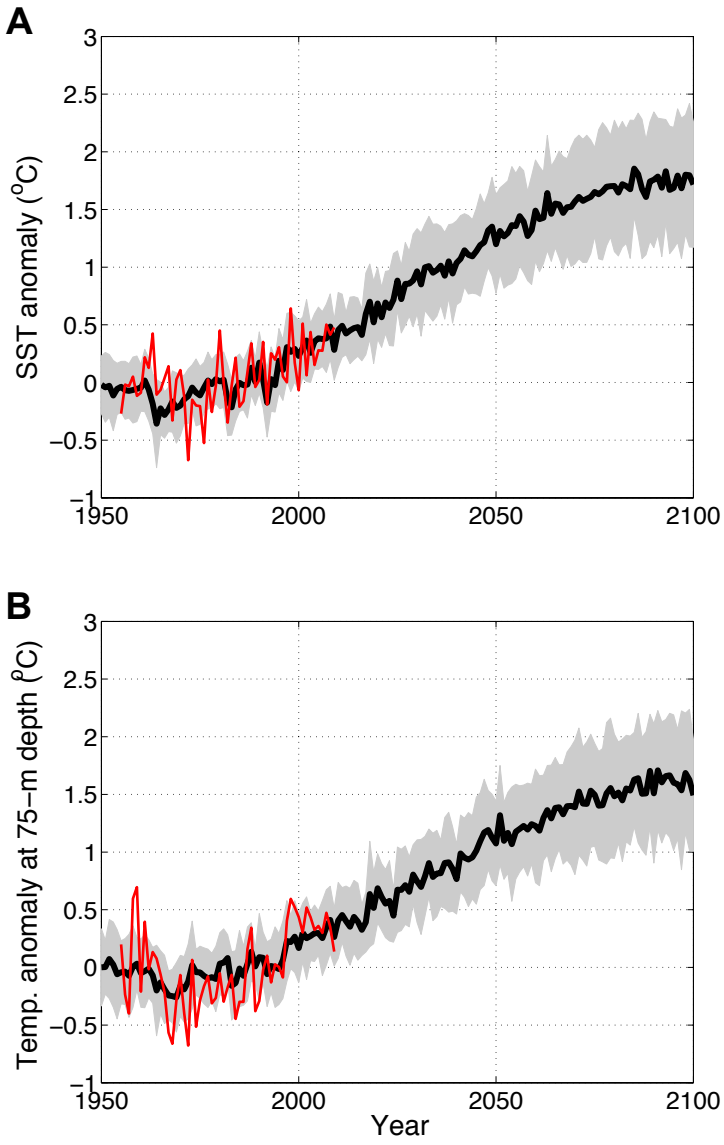

Fig. S7. **Observed and simulated changes in ocean temperatures.** Observed (red curve) and simulated (black curve) temporal evolution of temperature anomaly (in °C) at sea surface (A) and 75-m depth (B) averaged over the typhoon intensification region in the northwestern Pacific. The simulations are from 20 CMIP5 models and shading shows the spread of model results.

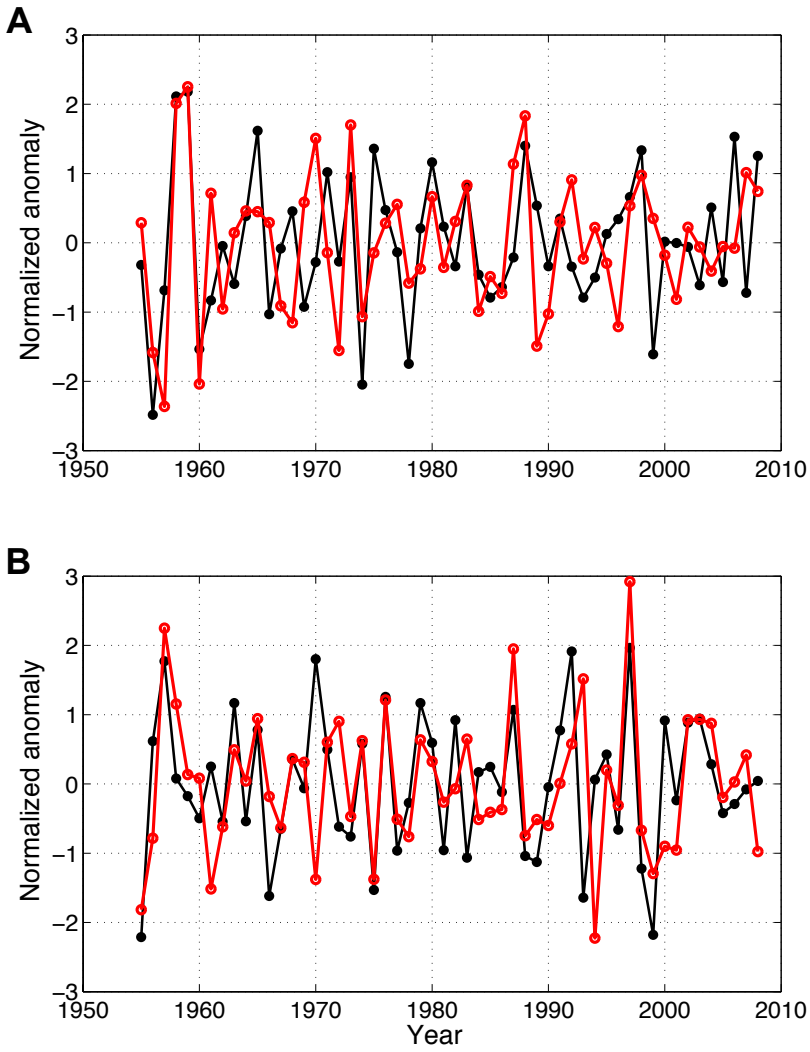

Fig. S8. **High-frequency variations in typhoon metrics and their modulation by oceanic and climate variables.** (A) Temporal evolution of normalized anomalies in 9-yr high-pass filtered intensification rate (black) and ocean temperature at 75-m depth averaged over the intensification region (red). The linear correlation coefficient between the two curves is 0.49 with a 95% confidence interval of [0.26 0.67]. (B) Temporal evolution of normalized anomalies in 9-yr high-pass filtered intensification duration (black) and PDO index (red). The linear correlation coefficient between the two curves is 0.47 with a 95% confidence interval of [0.24 0.66].

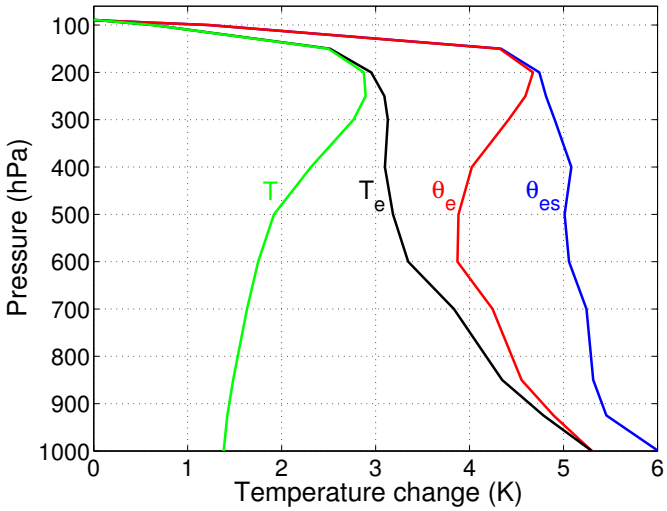

Fig. S9. **Simulated changes in various atmospheric thermodynamic variables.** Vertical profiles of changes in temperature T (green), equivalent temperature T_e (black), equivalent potential temperature θ_e (red), and saturated equivalent potential temperature θ_{es} (blue) averaged over the typhoon intensification region in the northwestern Pacific under RCP4.5 scenario by the end of this century.

Supplementary Tables

Table S1. **Correlation between the duration of typhoon intensification and various variables** [$\overline{\text{SST}}_{\text{trop}}$: global tropical mean SST (averaged between 20°S and 20°N); r_{upper} and r_{lower} respectively denote the upper and lower bounds for a 95% credible interval]

	U	φ_{end}-φ_{str}	λ_{end}-λ_{str}	φ_{str}	λ_{str}	φ_{end}	λ_{end}	Nino4	PDO	Nino4+PDO	$\overline{\text{SST}}_{\text{trop}}$
r	-0.30	-0.63	0.74	0.48	-0.45	0.34	-0.19	0.48	0.43	0.53	0.27
r_{upper}	-0.51	-0.76	0.84	0.65	-0.64	0.55	-0.43	0.66	0.61	0.69	-0.12
r_{lower}	-0.05	-0.44	0.60	0.25	-0.23	0.09	0.06	0.26	0.19	0.31	0.40

Table S2. Details of the ocean component of the CMIP5 models in use

Number	Model Name	Horizontal Resolution	Vertical Levels
1	ACCESS1.0	$1^\circ \times (1/4\text{-}1)^\circ$	50
2	BCC-CSM1.1	$1^\circ \times (1/3\text{-}1)^\circ$	40
3	BNU-ESM	$1^\circ \times (1/3\text{-}1)^\circ$	50
4	CanESM2	$1.4^\circ \times 0.9^\circ$	40
5	CCSM4	$1.11^\circ \times (0.27\text{-}0.54)^\circ$	60
6	CESM1-CAM5	$1.11^\circ \times (0.27\text{-}0.54)^\circ$	60
7	CNRM-CM5	$1^\circ \times (1/3\text{-}1)^\circ$	42
8	CSIRO-Mk3.6.0	$1.875^\circ \times 0.93^\circ$	31
9	GFDL-CM3	$1^\circ \times 1^\circ$	50
10	GISS-E2-R-CC	$1.25^\circ \times 1^\circ$	32
11	HadGEM2-CC	$1^\circ \times (1/3\text{-}1)^\circ$	40
12	HadGEM2-ES	$1^\circ \times (1/3\text{-}1)^\circ$	40
13	INMCM4	$1^\circ \times 0.5^\circ$	40
14	IPSL-CM5A-MR	$0.5^\circ \times 1^\circ$	31
15	IPSL-CM5B-LR	$0.5^\circ \times 1^\circ$	31
16	MIROC-ESM	$1.4^\circ \times 1^\circ$	44
17	MIROC4h	$0.28125^\circ \times 0.1875^\circ$	48
18	MPI-ESM-MR	$0.45^\circ \times 0.39^\circ$	40
19	MRI-CGCM3	$1^\circ \times 0.5^\circ$	51
20	NorESM1-ME	$1.125^\circ \times (0.26\text{-}0.64)^\circ$	70